

Transport of ultracold neutrons through a mirror system with surface roughness as a velocity filter

L.A. Chizhova,^{1,*} S. Rotter,¹ T. Jenke,² G. Cronenberg,² P. Geltenbort,³ H. Abele,² and J. Burgdörfer¹

¹*Institute for Theoretical Physics, Vienna University of Technology, 1040 Vienna, Austria, EU*

²*Institute of Atomic and Subatomic Physics, Vienna University of Technology, Stadionallee 2, 1020 Vienna, Austria, EU*

³*Institute Laue-Langevin, BP 156, 6, rue Jules Horowitz, 38042 Grenoble Cedex 9, France*

(Dated: December 5, 2012)

We perform classical Monte Carlo simulations of ultracold neutron transport through an absorbing-reflecting mirror system in the Earth's gravitational field. We show that the underlying mixed phase space of regular skipping motion and random motion due to disorder scattering can be exploited to realize a velocity filter for ultracold neutrons. The range of velocities selected is controlled by geometric parameters of the wave guide. Possible applications include investigations of transport and scattering dynamics in confined systems.

PACS numbers: 29.25.Dz, 25.40.Dn, 05.60.Cd, 05.45.-a

I. INTRODUCTION

Neutrons with an energy of around 100 neV or below are conventionally referred to as ultracold. One of their important properties is total reflection from many materials allowing for storage of ultracold neutrons (UCN) for long times up to their lifetime in material traps or sealed vessels. UCN are conveniently produced in a research reactor by extracting the low energy part of the Maxwellian spectrum of thermal neutrons and by directing them with neutron guides of different forms and sections [1, 2]. Well known applications of UCN include measurements of the neutron electric dipole moment [3, 4], the neutron half-life time [1, 2] as well as observation of the UCN quantum states in the Earth's gravitational field [5–8].

UCN can also serve as a powerful tool for studying quantum chaos [9], scattering of ultracold fermions [10, 11] and transport in confined geometries in the presence of only short-ranged interactions while eliminating distortions by Coulomb correlations and interactions. A major complication is, however, the loss of neutrons due to absorption by the confining material. The loss occurs primarily if the neutron velocity perpendicular to the boundary surfaces (v_{\perp}) exceeds a characteristic critical velocity (v_{cr}) for total reflection of the confining matter. Absorption is enhanced in wave guides with surface or bulk disorder as scattering at rough surfaces or impurities can increase v_{\perp} . The loss can be minimized by pre-selecting only such neutrons whose total velocity does not exceed the critical velocity of the waveguide walls. However, in the experiment without an additional selector such a condition is hard to achieve since the velocity spectra in the initial UCN beam usually shows nonzero probability of neutrons with velocities much larger than v_{cr} . In this paper we propose and simulate the efficiency of a band pass velocity filter for UCN. The proposed filter consists of a neutron absorbing-reflecting mirror setup

similar to the one used for the investigation of neutron quantum states [5, 7]. We focus on system parameters for which the system approaches the classical limit and quantum effects can be neglected. For sampling the classical phase space we employ the classical trajectory Monte Carlo (CTMC) method and derive analytic estimates for the velocity cut-offs of the filter.

II. SET-UP OF THE FILTER

Figure 1 shows a schematic picture of the proposed absorbing-reflecting mirror system (ARMS). The UCN beam from the neutron guide passing a collimator enters the ARMS which consist of two horizontal borosilicate glass plates, or mirrors, separated by a distance W . W is considered to be large enough ($W \gtrsim 160 \mu m$) to suppress quantum effects (such as diffraction and localization) and to allow for a classical transport description. The two glass plates are separated by two brass spacers which are rectangular blocks with height W and length

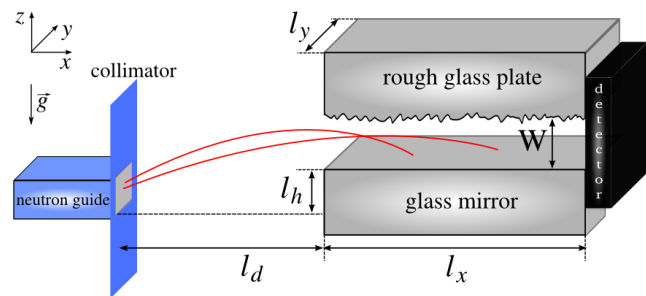


FIG. 1. Schematic view of ARMS proposed as the velocity filter consisting of a glass mirror (bottom) and a rough glass plate with surface disorder inducing large angle disorder scattering and absorption (top). The incident neutron beam leaves the neutron guide through a collimator. For the spacers position see Fig. 8(b).

* larisa.chizhova@tuwien.ac.at

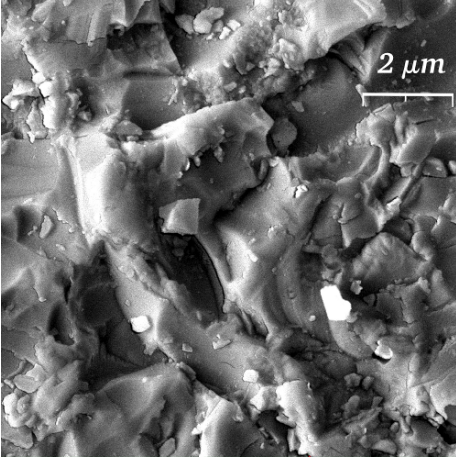


FIG. 2. A typical surface of the rough upper mirror coated with Ni measured with the scanning electron microscope. (The measurement was performed at the USTEM facility [14].) The disorder has amplitude $A \sim 3 \mu\text{m}$ and a correlation length $l_{cor} \sim 2 \mu\text{m}$.

equal to the mirror length l_x (see Fig. 8(b), not shown in Fig. 1) placed symmetrically at the sides of the glass plates. The inner surface of the *upper* mirror is rough where the roughness is characterized by the amplitude A of the disorder and its correlation length l_{cor} . A typical surface profile measured with a scanning electron microscope is shown in Fig. 2. The inner surface of the *lower* mirror is flat allowing for specular reflections. Only the neutrons which pass through this device without being absorbed by the glass plates (or by the spacers) are detected. The detector covers an area of $W \times l_y$ (Fig. 1).

To understand how this device can operate as a velocity filter, we analyze the classical phase space of this system with mixed regular-chaotic dynamics. A neutron traveling between two mirrors has 3 degrees of freedom and its Hamiltonian is given by

$$H(p_x, p_y, p_z, x, y, z) = \frac{p_x^2}{2m} + \frac{p_y^2}{2m} + \frac{p_z^2}{2m} + mgz + V(x, y, z), \quad (1)$$

where g is the Earth's gravitational constant and $V(x, y, z)$ describes the potential of the walls approximated by:

$$V(x, y, z) = \begin{cases} 0, & \text{if } 0 < z < \xi(x, y) \\ V_F, & \text{otherwise,} \end{cases} \quad (2)$$

where $\xi(x, y)$ describes the disorder landscape of the upper disordered surface and V_F will be discussed later. The Hamiltonian in Eq. (1) governs the trajectories in 6-dimensional phase space. A useful method for the visualization of trajectories lying on the 5-dimensional isoenergy surface in multi-dimensional phase space is the projected Poincaré surface of section. We start from a four-dimensional surface of section given by a cut at the system exit $x = l_x$ with periodic boundary condition in x

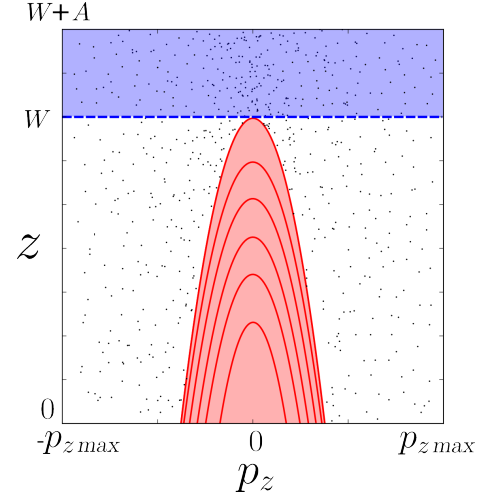


FIG. 3. The projection of the Poincaré surface of section on the (p_z, z) plane of the phase space for neutron transport consists of a regular island (red area at the center) representing skipping trajectories, and of an irregular part of scattering trajectories induced by the surface disorder with roughness amplitude A . The blue area with z ranging from W to $W + A$ indicates the region where neutrons scatter off the upper surface.

direction. We then project the surface of section onto the (p_z, z) plane for $p_x > 0$. Fig. 3 clearly displays two types of motion (note that due to time-reversal symmetry the surface of section for $p_x < 0$ is equivalent). The large regular island at the center corresponds to the neutrons repeatedly bouncing off the lower mirror in the Earth's gravitational field (*skipping* motion, [12]) and traveling through the filter without touching the upper rough wall. For this motion the degrees of freedom are separable and the trajectory intersection lies on a smooth curve in the (p_z, z) plane. The equation for this curve $p_z = p_z(z)$ follows from the Hamilton equation with the Hamiltonian $H(p_z, z) = H_{z0}$ being the integral of motion and independent of the other two degrees of freedom:

$$p_z = \pm m \sqrt{2g(h - z)}, \quad (3)$$

where h is a maximal height that a neutron can achieve for a given energy $H_{z0} = mgh$. The region of skipping motion in phase space is in contrast to the region of *chaotic* motion of those neutrons that scatter off the disordered upper surface creating the chaotic sea in phase space. In the latter case, due to the roughness, the degrees of freedom are not separable and additional integrals of motion, besides the total energy, no longer exist. Therefore, the intersection of randomly scattered trajectory with the projected surface of section does not form smooth curve and shows chaotic behavior instead [15].

The interaction of neutrons with the surface of the glass walls as well as the spacers is described by a Fermi pseudopotential V_F which characterizes the low-energy nuclear scattering of surface atoms [1, 2] and can be writ-

ten as

$$V_F = V_R - iV_I = \frac{2\pi\hbar^2}{m}N(b - ib_i), \quad (4)$$

where m is the neutron mass, N is the scattering center density, b is the coherent nuclear scattering length, and the imaginary part of the potential is determined by

$$b_i = \frac{\sigma_l v}{4\pi\hbar}, \quad (5)$$

where v is the neutron velocity and σ_l is the absorption scattering cross section due to the interaction of neutrons with nuclei of surface atoms. The absorption results from neutron capture by nuclei accompanied by emission of γ -rays or charged particles. This effect is accounted for within our description of elastic neutron transport by introducing the effective imaginary potential V_I in (4). Within the classical simulation, it gives rise to a loss probability for the trajectories.

The real part of the Fermi potential V_R determines the critical energy and velocity v_{cr} of neutrons which are reflected. If a neutron has a kinetic energy in the direction normal to the surface larger than the real part of the Fermi potential of the surface material ($E_\perp > V_R$), it penetrates the wall and is considered to be lost. The surface roughness gives rise to nonspecular reflection and, thus, to transfer of longitudinal (E_\parallel) to transverse (E_\perp) energy of neutrons. As a result, the total absorption will be enhanced by surface disorder. Consequently, neutrons scattered off the upper wall, i.e. neutrons undergoing chaotic scattering are effectively removed from the transmission.

Even for $E_\perp < V_R$ the reflection probability from the mirror surfaces is below one, due to an exponential penetration of the wave function into the barrier ("tunneling"). The reflection probability of the neutron from the step-like potential barrier follows as (e.g. see [2, 16])

$$R = \left(\frac{k_0 - k}{k_0 + k} \right)^2 = \left(\frac{E_\perp^{1/2} - (E_\perp - V_F)^{1/2}}{E_\perp^{1/2} + (E_\perp - V_F)^{1/2}} \right)^2, \quad (6)$$

where k_0 and k are the normal components of the wave vector in vacuum and in the medium. For the case $V_I \ll V_R$ (usually V_I is 10^4 times smaller than V_R) the reflection coefficient, to first order in V_I/V_R , becomes [2]:

$$R = 1 - \mu(E_\perp) = 1 - 2 \frac{V_I}{V_R} \sqrt{\frac{E_\perp}{V_R - E_\perp}} \quad (7)$$

with $E_\perp < V_R$. The wall-loss probability per bounce is denoted by $\mu(E_\perp)$. It should be noted that $V_I/V_R = \sigma_l v / 4\pi\hbar b$ is independent of the neutron velocity since σ_l is proportional to $1/v$ [1]. Multiple scattering leads to preferential depletion of the chaotic region of the phase space since the number of bounces at walls for chaotic scattering trajectories is much larger than for skipping trajectories.

III. MONTE CARLO SIMULATION

To explore the implications of the phase space structure analyzed above for the neutron transport through the ARMS, we perform a full three-dimensional Monte Carlo simulation using the geometric parameters of typical set-ups and realistic initial distributions of the neutron beam.

A. Geometry of the set-up

The two parallel absorber-mirrors are chosen to be square plates with $l_x = l_y = 10 \text{ cm}$ (see Fig. 1). To stay within the classical regime the distance between the two mirrors is selected to be $W = 250 \mu\text{m}$, in agreement with experiments (see, e.g. [5]). The mirrors are made of borosilicate glass and have a critical velocity $v_{cr} = 4.3 \text{ m/s}$ and a loss factor (see Eq. (7)) of $V_I/V_R = 0.0015$ [1]. The brass spacers (see Fig. 8(b)) have a critical velocity $v_{cr} = 5.3 \text{ m/s}$ [1]. To simulate the landscape of surface disorder $\xi(x, y)$ in Hamiltonian in Eq. (1) with realistic spatial correlations we use a convolution method with a Gaussian correlation function:

$$\langle \xi(x, y) \xi(x + x', y + y') \rangle = A^2 \exp\left(-\frac{x'^2}{2l_{cor}^2}\right) \exp\left(-\frac{y'^2}{2l_{cor}^2}\right). \quad (8)$$

The description of this method can be found in [17, 18]. The amplitude and the correlation length of the surface disorder in the simulations are chosen to be $A = 3 \mu\text{m}$ and $l_{cor} = 2 \mu\text{m}$ taken from the measured surface profile (Fig. 2). The distance between collimator and mirrors is $l_d = 18 \text{ cm}$, the distance between the lower collimator edge and the lower mirror surface is $l_h = 5.4 \text{ mm}$. The size of the collimator opening is $y \times z = 8 \text{ cm} \times 2.7 \text{ mm}$. We emphasize that the present simulation of the two-mirror setup taking into account also the transverse degree of freedom y is fully 3D unlike earlier two-dimensional models for similar systems [7, 13].

B. Initial conditions

The simulation requires the phase space distribution $\rho(\vec{r}, \vec{v}, t = 0)$ of the UCN beam as it exits the collimator as initial conditions for the propagation. The most reliable information about the distribution of the forward velocity component v_x of the neutron beam at the exit of the neutron guide can be obtained from time-of-flight (TOF) measurements. In such a measurement, the neutron beam is periodically chopped (see, e.g. [19]). After this chopper, the neutrons traverse a neutron guide of known length before they are detected with the help of a neutron counter. The detector electronics also receives one logical signal per turn of the chopper blade and thereby measures the time of flight of the neutrons.

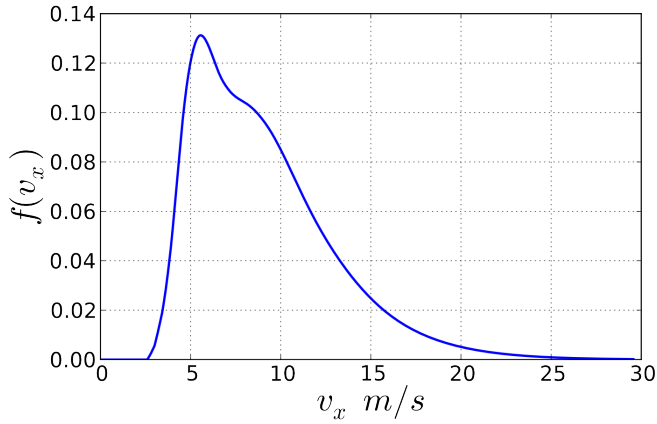


FIG. 4. Velocity distribution $f(v_x)$ measured by time-of-flight at the ILL facility for a straight, 2 m long cylindrical neutron guide with 4 cm radius.

The time-of-flight spectrum of the ultracold neutron beam at the Institute Laue-Langevin was measured with this method in 2008 [20]. The time-of-flight spectrum was corrected for the chopper offset. The opening function of the chopper was deconvoluted and with the help of the distance-of-flight, the corresponding velocity spectrum was extracted. The resulting normalized distribution of the forward velocity in x -direction (Fig. 4) will be used as initial distribution function.

Although it is difficult to measure the transverse velocity components v_y and v_z , part of the angular distribution $P(\theta)$ of the beam are available (see, e.g. [1, 21]). $P(\theta)$ depends on the ratio R of length to radius of the neutron guide. Since the angular distribution for the pipe which was used for the TOF measurement is unknown we perform our calculations for two distributions which correspond to the following limiting cases: in case of the ratio $R \gg 1$ the angular distribution is well approximated by $P(\theta) \sim \cos(\theta)$ and in case of a short pipe with $R \lesssim 1$ the angular distribution is uniform. Because of the cylindrical symmetry of the pipe and the small angles involved, we consider the distributions $P(\theta_y)$ and $P(\theta_z)$ to be identical and either cosine or uniformly distributed. Since the inner surface of the cylindrical neutron guide is coated with Ni^{58} , which has a critical velocity of 8.07 m/s, the velocity component normal to the guide surface at the pipe exit $v_\perp = \sqrt{v_y^2 + v_z^2}$ should be less than 8.07 m/s. The initial vectorial velocity distribution is randomly sampled from these distributions. The coordinate distribution of the neutron beam in the plane of the collimator opening is assumed to be uniform.

C. Simulation results

The classical equations of motion are integrated for a large number of initial conditions $\rho(t=0)$. Calculations start at the collimator opening with initial conditions

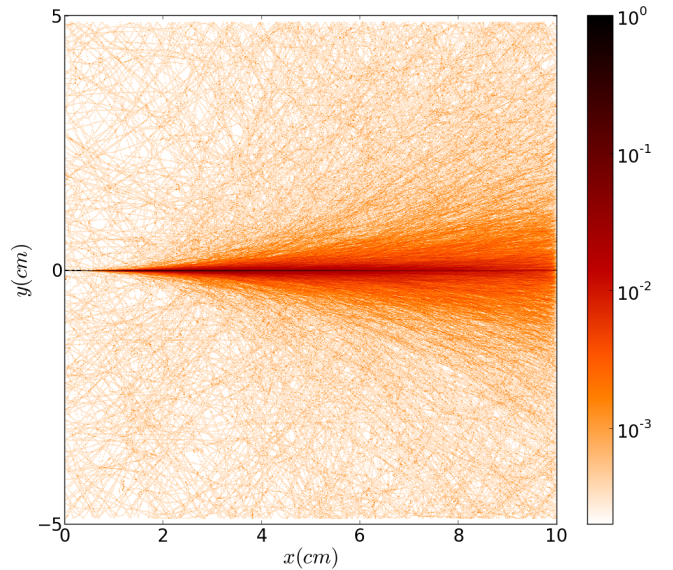


FIG. 5. A sample distribution of 3000 trajectories undergoing chaotic scattering in the top view of the absorbing-reflecting mirror system (ARMS). The trajectories enter with initial conditions $y = 0$ and $v_y = 0$. Color scale in arbitrary units.

randomly selected for each particle from the distributions discussed in section III B. The number of neutrons that reach the mirror slit entrance is kept fixed at $5 \cdot 10^5$ for the results presented in this section. The propagation inside the slit includes absorption by walls and by spacers when the kinetic energy perpendicular to the surface is larger than the Fermi potential. The wall-loss probability per bounce Eq. (7) is included as a stochastic process for each collision with the wall. An example of the trajectory distribution between two mirror plates in top view of the system is shown in Fig. 5. The trajectories depicted here are calculated for 3000 different initial conditions lying inside the region of chaotic scattering. For better visualization we restricted here the initial conditions to $y = 0$ and $v_y = 0$. We also do not show the skipping trajectories as they would coalesce to a single line ($y = 0$, in this case) and would decrease the contrast of the irregular scattering pattern.

Results of the classical Monte Carlo simulations of the full 3D filter system are presented in Fig. 6, where distributions $f(v_i)$ of the absolute value of the total velocity (a) as well as the v_x , v_y and v_z velocity components (c-d) at the detector position are shown for an initial cosine angular distribution. If a uniform initial angular distribution in the beam is used instead, the results hardly differ from the ones presented in Fig. 6. This is a consequence of the fact that the initial maximal angles are rather small ($\theta_y \sim 26^\circ$ and $\theta_z \sim 7^\circ$). Therefore, the uniform and cosine distributions do not significantly differ from each other.

The Poincaré surface of section $x = l_x$ in the phase space projected on the (v_z, z) plane for the case of a cosine angular distributions (Fig. 7(a)) prominently dis-

plays a regular island of skipping motion with dense non-uniform distribution. The distribution of the chaotic scattering trajectories is barely visible in this plot since they spread out on a much larger region in phase space.

D. Analytic estimate of the velocity band pass

Each velocity component distribution can be decomposed into contributions from skipping and chaotic scattering trajectories (blue dotted and green dashed lines in Fig. 6). For the skipping part of phase space it is possible to provide an analytical estimate for the velocity range, i.e. the minimum and maximum velocity of neutrons that can pass the filter. The shape of the distributions is more difficult to estimate since it strongly depends on the initial velocities in the neutron beam. However, the velocity limits are independent of the initial distribution (provided it lies within the skipping region of phase space).

The band pass in forward direction, v_x , can be calculated as follows. The maximum (minimum) velocity corresponds to the minimum (maximum) time of flight between the collimator and the glass mirrors

$$t_x = l_d / v_x. \quad (9)$$

Moreover, neutrons have to enter the mirror system in the skipping region: neutrons do not touch the upper rough surface if the vertical velocity component at the collimator lies in the interval

$$\sqrt{2g\delta z} \leq v_{z0} \leq \sqrt{2g(\delta z + W)}, \quad (10)$$

where δz is the distance between the lower glass plate and an initial z -coordinate of the neutron at the collimator opening. Taking into account the motion in z direction allows to calculate the neutron time of flight between the collimator and the glass mirrors (Eq. (9)),

$$t_{\perp} = (v_{z0} - v_{zs})/g, \quad (11)$$

where $v_{z0} = v_z(t=0)$ is the initial vertical velocity and v_{zs} is the velocity component at the mirror entrance slit,

$$v_{zs} = \pm \sqrt{v_{z0}^2 - 2g(\delta z + z_{sl})}. \quad (12)$$

Here z_{sl} is the vertical distance from the point where the trajectory enters the ARMS to the lower mirror. Eq. (9) and Eq. (11) gives v_x as a function of v_{z0} and δz

$$v_x = \frac{gl_d}{v_{z0} \pm \sqrt{v_{z0}^2 - 2g(\delta z + z_{sl})}}. \quad (13)$$

For the fastest (slowest) neutrons the denominator in Eq. (13) has the smallest (largest) value corresponding to the $- (+)$ sign. Also, the absolute value of v_{zs} in Eq. (12) should be maximal which is reached for $z_{sl} = 0$ and v_{z0} at its maximum value obtained from Eq. (10). In addition

δz takes on the smallest (largest) possible value. The two trajectories with maximal and minimal v_x are illustrated in Fig. 8(a) (side view) and correspond to the velocities

$$v_{xmax} = \frac{gl_d}{\sqrt{2g(\delta z_{up} + W)} - \sqrt{2gW}},$$

$$v_{xmin} = \frac{gl_d}{\sqrt{2g(\delta z_{down} + W)} + \sqrt{2gW}}, \quad (14)$$

where δz_{up} (δz_{down}) is the distance between the upper (lower) edge of the collimator opening and the lower glass plate (see Fig. 8(a)). Eq. (14) represents the analytic estimate for the velocity band pass for v_x . Obviously, the velocity range in Eq. (14) is controlled only by geometric parameters of the system and can be tuned accordingly.

The range of transmitted vertical velocity component v_z for trajectories undergoing skipping motion can be obtained from the requirement that neutrons do not touch the upper wall inside the mirror slit, i.e.,

$$|v_z| \leq \sqrt{2gW}. \quad (15)$$

The range of the v_y component can be found from Fig. 8(b) representing the top view of the system. Here the trajectories with the largest angles that can still be detected are shown. In the presence of spacers we find

$$|v_y| \leq v_{xmax} \frac{l_y + l_{yc}}{2l_d}, \quad (16a)$$

where l_{yc} is the size of the collimator opening in y -direction. Without spacers the allowed velocity range is reduced to

$$|v_y| \leq v_{xmax} \frac{l_y + l_{yc}}{2(l_d + l_x)}, \quad (16b)$$

since neutrons that would have been reflected from the spacers and stay inside the system are now lost. The v_y range depends also only on the geometric parameters of the system and can be tuned as well.

The limits Eq. (14 - 16) are depicted in Fig. 6(b-d) as dashed vertical lines and coincide with limits for the distributions of the skipping states (blue dotted lines) obtained from Monte Carlo simulations. It should be noted that the band pass filter limits for the v_x and v_z velocity components are separable, i.e. independent of the other Cartesian components of the velocity vector and only controlled by geometry. Only the v_y limit depends, in addition to geometric parameters, on the maximum velocity in x direction. Consequently, the ARMS can serve as a band pass filter for the full vectorial velocity \vec{v} , however only for skipping motion.

It is now crucial to inquire the relative importance of skipping compared to chaotic trajectories and gather parameters to enhance the relative weight of the skipping region of phase space for which the filter is operational. For the case depicted in Fig. 6, the fraction of chaotic scattering trajectories

$$F_c = \frac{\Gamma_c}{\Gamma_c + \Gamma_s}, \quad (17)$$

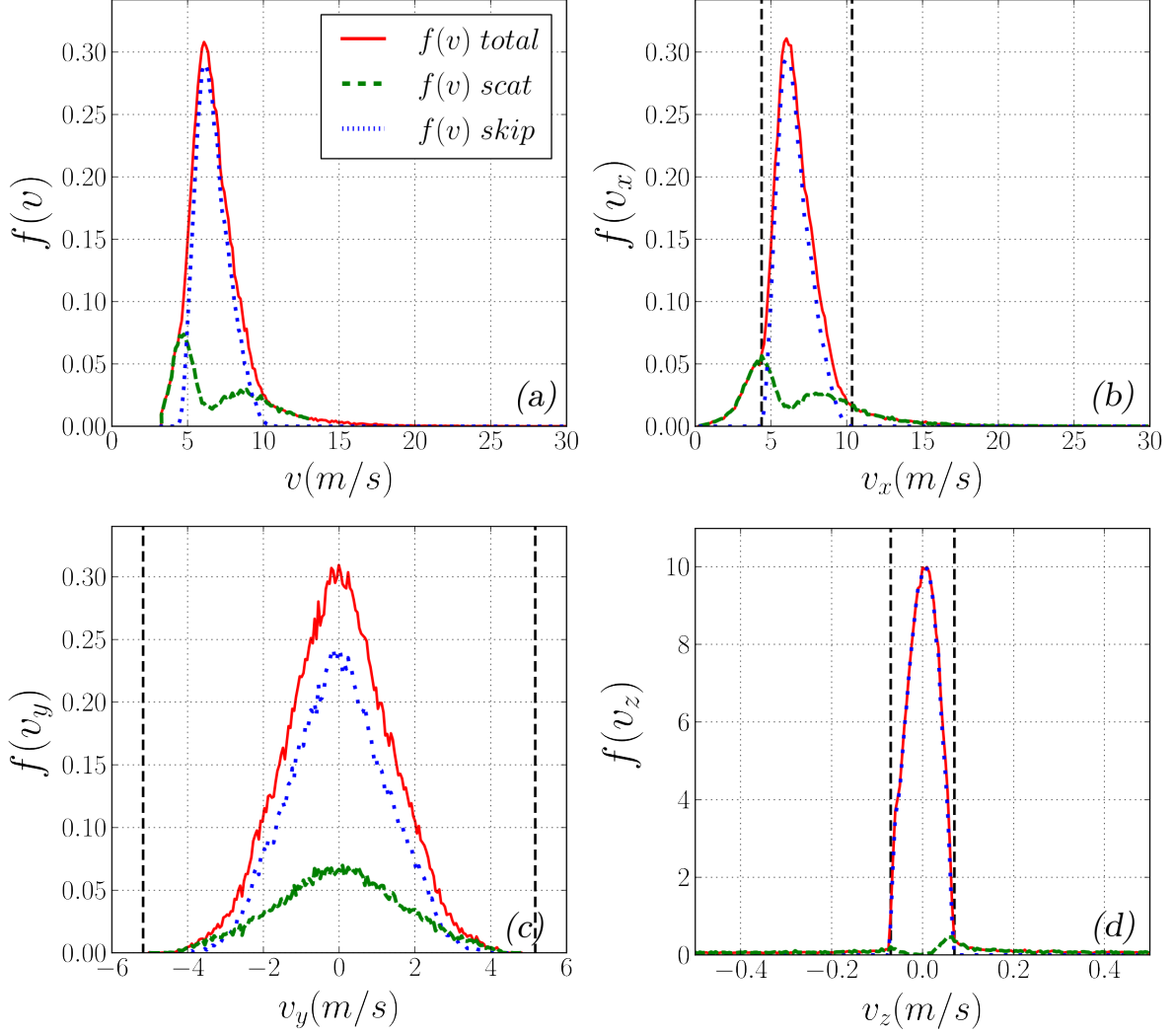


FIG. 6. Monte Carlo simulations for the components of the vectorial velocity distribution after passing the ARMS with parameters discussed in section III A. (a) Distribution of the absolute value of the total velocity $f(v)$; (b-d) distributions of the components $f(v_x)$, $f(v_y)$ and $f(v_z)$. The total distributions (solid red lines) can be decomposed into gravitational skipping (dotted blue line) and chaotic scattering (dashed green line) trajectories. Vertical lines correspond to analytical results for the band pass of the velocity components Eq.(14-16). The parameters of the filter: $W = 250 \mu m$, $l_x = l_y = 10 cm$, $A = 3 \mu m$, $l_{cor} = 2 \mu m$.

where $\Gamma_{c,s}$ denotes the volume in phase space pertaining to either chaotic (c) or skipping (s) motion, is $F_c = 0.27$. This fraction can, however, be tuned (see Fig. 9) by exploiting the fact that chaotic trajectories executing many random bounces at the mirror are subject to enhanced absorption (see Eq. (7)). For example, for the distributions of Fig. 6, the absorption by wall collisions suppresses the flux of chaotic scattering trajectories at the detector by 12%. In contrast, the flux of neutrons undergoing skipping motion is reduced only by 0.2%, because of the drastically different number of collisions for chaotic scattering and skipping motion (for this example ~ 500 and ~ 10 , respectively). By further increas-

ing the number of bounces the phase space region associated with chaotic scattering can be even more suppressed. Trajectories belonging to Γ_c give rise to a broad velocity distribution at the detector extending well beyond v_{cr} and the band pass (Eq. (14-16), see Fig. 6). The low-velocity portion corresponds to trajectories with a large number of bounces. Since the total velocity of these neutrons is less than v_{cr} they do not penetrate the walls. The leading loss mechanism is given by Eq. (7) which reduces the number of these neutrons but does not completely remove them. A simple estimate for reflection losses (without taking into account the angular dependencies) is $\sim \exp(-N^{V_I}/V_R)$, where N is number of

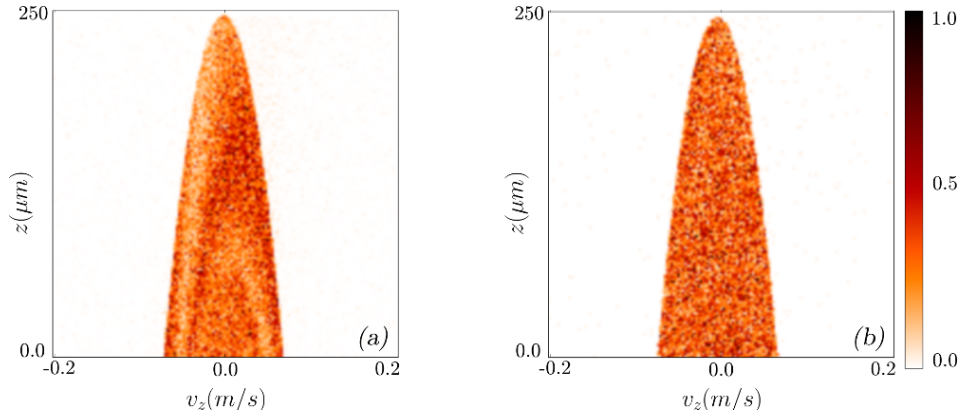


FIG. 7. Projection of the Poincaré section $x = l_x$ on the (v_z, z) plane for the filter system with (a) $l_x = 0.1$ m and (b) $l_x = 0.2$ m. Only the regular island is visible since the trajectories in the chaotic sea are spread out over a large volume in the phase space resulting in a much reduced density in the projected surface of section compared to the regular island.

bounces and $V_I/V_R = 0.0015$. Strongly suppressing the amount of these low-velocity neutrons would require ~ 2000 and more wall collisions. The high velocity part of the spectrum corresponds to neutrons undergoing only a few collisions with the rough wall. The normal velocity, v_\perp , remains still less than v_{cr} allowing these particles to

travel through the mirror system without being lost.

One more aspect to be discussed is the influence of spacers. Our Monte Carlo simulations indicate that 34% of the total number of trajectories (24% from skipping motion and 10% from scattering motion) are reflected from the spacers. We consider spacers to be flat and to be perfect specular reflectors, i.e. only v_y changes sign after scattering. Realistically the spacers do have a rough surface as well as other surface imperfections and thus may also give rise to randomization of the reflection angle. This can lead to an additional contribution to the irregular part of phase space. For example, skipping trajectories can become chaotic scattering trajectories after a single reflection from a spacer. Thus, in the following we focus on the system without spacers.

E. Suppression of chaotic scattering contribution

Controlling chaotic scattering trajectories requires the tuning of the surface disorder and the length of the mirror system. In particular, the chaotic part of the phase space F_c can be suppressed by increasing the number of wall collisions as it was discussed in section III D. Enhancing the number of bounces is accomplished by either increasing the length l_x or decreasing the width W . Furthermore, a variation of the amplitude A and correlation length l_{cor} allows to modify the number of wall collisions and, moreover, to control scattering into states with $v_\perp > v_{cr}$.

The sensitivity to the variation of the available control parameters is shown in Fig. 9. While the fraction of chaotic phase space F_c strongly decreases with l_x , the variation with W is much weaker. Accordingly, F_c does not simply scale with W/l_x . This is, in fact, due to the presence of additional relevant length scales, A and l_{cor} . F_c and, thus, the chaotic scattering contribution outside of the filter band pass can be minimized for a long mirror system (large l_x) with short-ranged surface disorder

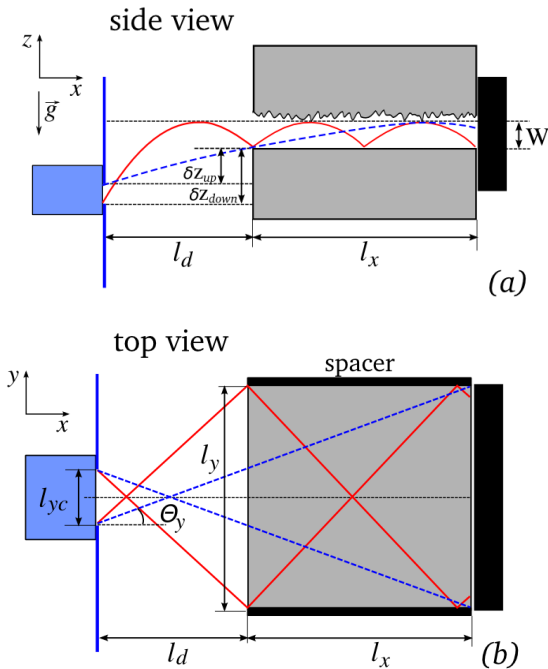


FIG. 8. Trajectories representing the limiting velocities for transmission. (a) the v_x component, the solid red line corresponds to the trajectory with minimal forward velocity, the dashed blue line to the one with maximal v_x . (b) the v_y component, the solid red line corresponds to the trajectory launching with the largest angle θ_y still reflected by the spacers (depicted as black horizontal rectangles), the dashed line displays the same in case without spacers.

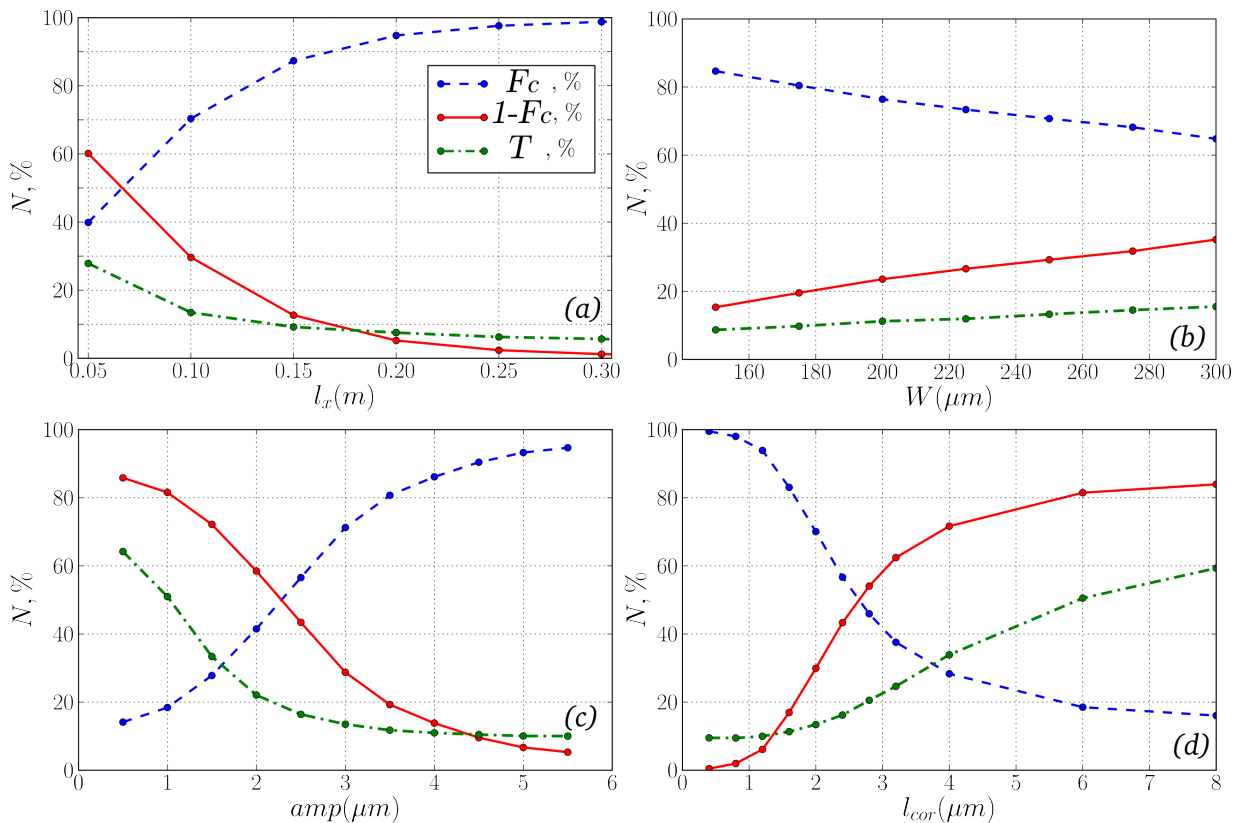


FIG. 9. Dependence of the fraction of chaotic scattering F_c (solid line), skipping ($1 - F_c$) (dashed line) trajectories and the total transmission probability T through the neutron filter (dotted-dashed line) as a function of (a) the filter length l_x ; (b) of the slit width W ; (c) of the amplitude A and (d) of the correlation length l_{cor} of the surface disorder. The parameters of the filter (if not varying): $W = 250 \mu m$, $l_x = l_y = 10 cm$, $A = 3 \mu m$, $l_{cor} = 2 \mu m$.

(small l_{cor}) and large disorder amplitude A . Clearly, the price to pay for this purification of the beam is the reduction of the overall transmission probability (typically $\lesssim 10 \%$).

Since a variation of the amplitude or the correlation length of the surface disorder might be experimentally difficult to achieve, a practical approach is to vary the length of the mirrors. In Fig. 10 we present distributions of the total velocity and its Cartesian components v_x , v_y and v_z in the absence of the spacers and for the doubled length ($l_x = 20 cm$) of the ARMS compared to the previous settings (Fig. 6). The initial angular distributions entering the CTMC simulation are, as before, cosine distributions (results for uniform distributions are hardly different).

In the data shown in Fig. 10, contribution from chaotic scattering trajectories to the velocity distributions is suppressed and the spectra consist predominantly of skipping trajectories (see Fig. 6 for comparison). Although the high velocity part of the spectra (see Fig. 10(a, b)) outside the upper filter limit has disappeared, there is still a small contribution of chaotic scattering trajectories at velocity below the lower cut-off of the filter. This part corresponds to neutrons with an energy smaller than the Fermi potential of the mirrors and with a number

of bounces not high enough to be absorbed due to repeated wall collisions. Because of an increasing number of bounces the distribution within the regular island at the detector position, shown in Fig. 7(b), becomes more homogeneous compared to Fig. 7(a). From the fraction of the total number of detected neutrons (Fig. 9(a)), it can be seen that the accumulation time for good statistics is of the same order as for the setup previously discussed in section III A.

IV. CONCLUSION

In the present work, we propose and analyze an absorbing-reflecting mirror system which can be used as velocity band pass filter for ultracold neutrons. Full three-dimensional Monte Carlo simulations of the propagation of UCN through the system have been performed. The efficiency of the filter is explored as a function of the geometric control parameters and the underlying scattering phase space structure is analyzed.

Due to the mixed phase space, there are two types of motion in the system: the regular skipping motion which corresponds to the trajectories bouncing off the lower wall only and chaotic scattering trajectories which scat-

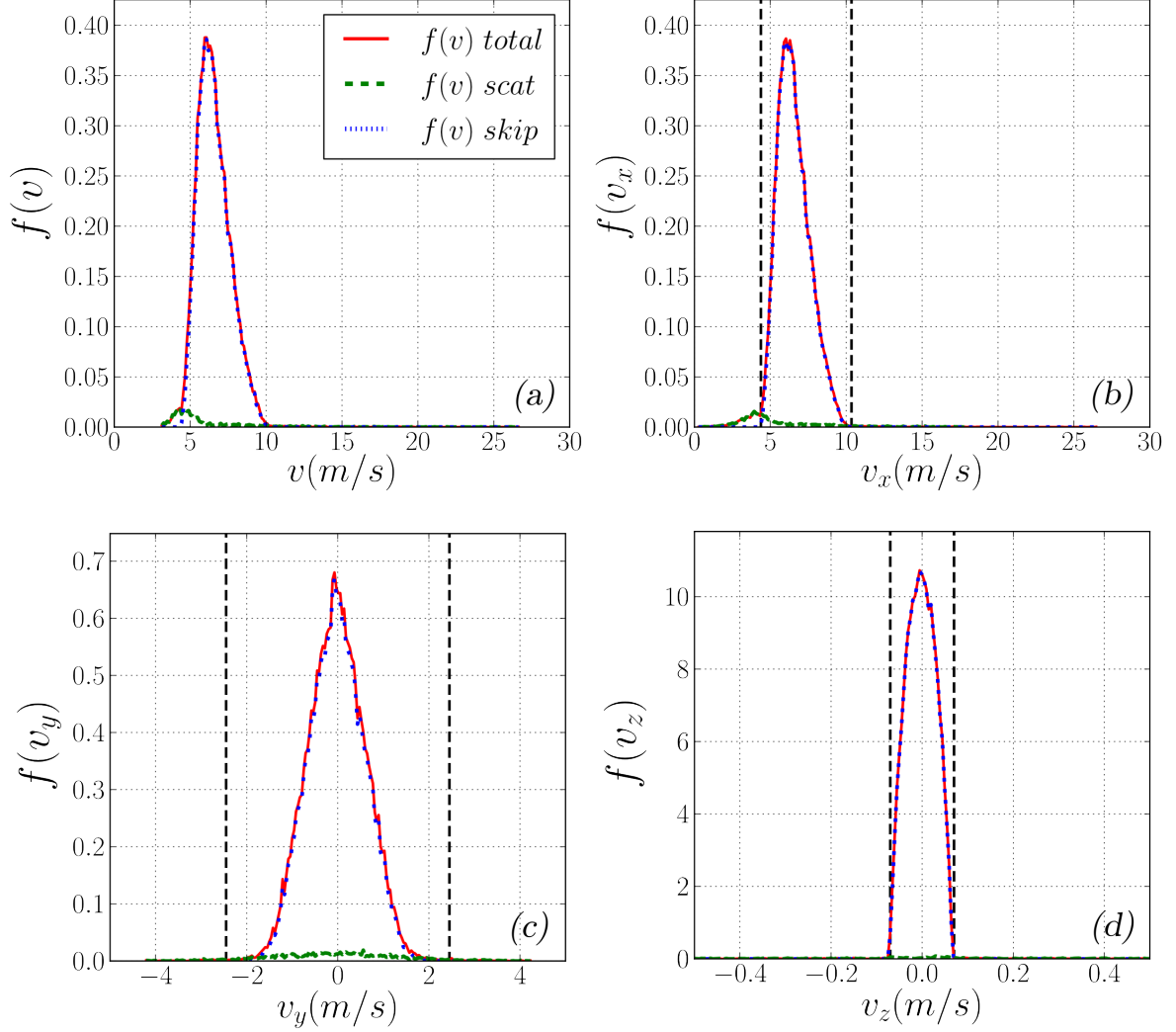


FIG. 10. Classical trajectory Monte Carlo simulations for the filter as in Fig.(6), however with doubled length $l_x = 20$ cm and without spacers. Distributions of: (a) the absolute value of the total velocity $f(v)$; (b-d) the velocity components $f(v_x)$, $f(v_y)$ and $f(v_z)$ (solid line). Contributions from gravitational skipping and chaotic scattering trajectories are indicated by dotted blue and dashed green lines, respectively. Vertical lines correspond to analytical results for the velocity band pass (see Eq.(14-16)). The parameters of the filter: $W = 250 \mu\text{m}$, $l_y = 10$ cm, $A = 3 \mu\text{m}$, $l_{cor} = 2 \mu\text{m}$.

ter also off the upper plate with surface disorder. These different classes of motion give different contributions to the total velocity distribution of the detected neutrons. Since skipping motion is regular and well controlled, the transmission is allowed only for a limited window of the full vectorial velocities giving rise to a band pass filter. Its limits can be determined analytically. They depend only on the geometric parameters of the system and are independent of the initial velocity distributions at the exit of the neutron guide which are usually only partly known.

The second part of the total velocity spectrum consists of neutrons coming from the irregular part of the phase space. The fraction of such neutrons strongly depends

on the number of scattering events inside the mirror slit. This contribution extends over the whole range of velocities available at the collimator including those with high, unwanted velocities. That is why in experiments in which a limited velocity range is important, it is necessary to suppress the fraction of such chaotic scattering trajectories. We have shown that by optimizing the geometric parameters of the filter or the surface disorder the fraction of neutrons arriving at the detector originating from the chaotic sea of the phase space can be reduced to 5% (or less) of the total number of the detected neutrons. The proposed system delivers the neutrons coming mostly from the regular island with a well-defined velocity range while suppressing the trajectories from the

irregular part of the phase space. We expect the application of such a filter system to UCN experiments on quantum scattering phenomena [22] in the near future.

ACKNOWLEDGMENTS

We gratefully acknowledge support by the doctoral colleges CMS (TU-Vienna) and Solids4Fun (FWF), by the

SFB ViCom (FWF-SFB 041), by the Austrian Science Fund (FWF) under Contract Nos. I592-N20 and I862-N20, by the German Research Foundation (DFG) as part of the Priority Programme (SPP) 1491 “Precision experiments in particle and astrophysics with cold and ultracold neutrons” as well as by the French Science Fund (ANR) under contract number ANR-2011-ISO4-007-02, Programme Blanc International - SIMI4-Physique.

-
- [1] V.K. Ignatovich, *The Physics of Ultracold Neutrons* (Clarendon Press, Oxford, 1990).
 - [2] R. Golub and J.M. Pendlebury, Rep. Progr. Phys. **42**, 439 (1979).
 - [3] C.A. Baker, D.D. Doyle, P. Geltenbort et al., Phys. Rev. Lett. **97**, 131801 (2006).
 - [4] J. Beringer et al. (Particle Data Group), Phys. Rev. D **86**, 010001 (2012).
 - [5] V.V. Nesvizhevsky, H.G. Börner, A.K. Petukhov et al., Nature **415**, 297 (2002).
 - [6] V.V. Nesvizhevsky et al., Eur. Phys. J. C **40**, 479 (2005).
 - [7] A. Westphal, H. Abele, S. Baekler, et al., Eur. Phys. J. C **51**, 367 (2007).
 - [8] T. Jenke, P. Geltenbort, H. Lemmel and H. Abele, Nature Physics **7**, 468 (2011).
 - [9] H.J. Stöckmann, *Quantum chaos* (Cambridge University Press, 1999).
 - [10] U. Schneider, L. Hackermüller, J.P. Ronzheimer et al., Nature Physics **8**, 213 (2012).
 - [11] J.-P. Brantut, J. Meineke, D. Stadler, S. Krinner and T. Esslinger, Science **337**, 1069 (2012).
 - [12] Y.H. Ohtsuki, K. Koyama and Y. Yamamura, Phys. Rev. B **20**, 5044 (1979).
 - [13] A.E. Meyerovich and V.V. Nesvizhevsky, Phys. Rev. A **73**, 063616 (2006).
 - [14] Universitäre Service - Einrichtung für Transmissions - Elektronmikroskopie, Vienna University of Technology, <http://www.ustem.tuwien.ac.at/EN/>
 - [15] A.J. Lichtenberg and M.A. Lieberman, *Regular and Chaotic Dynamics* (Springer-Verlag, 1992), second ed.
 - [16] L.D. Landau and E.M. Lifshitz, *Quantum mechanics. Non-relativistic theory*, (Pergamon Press, 1977), third ed., p. 78
 - [17] S.O. Rice, in *Mathematical Analysis of Random Noise, Selected Papers on Noise and Stochastic Processes*, edited by N. Wax (Dover, New York, 1954), p. 180
 - [18] F.M. Izrailev, N.M. Makarov, in *Structured Surfaces as Optical Metamaterials*, edited by A.A. Maradudin (Cambridge University Press, 2011), p. 283-311
 - [19] A. Fierlinger, A. Pichlmaier and H. Rauch, Nucl. Instr. and Meth. in Phys. Res. A **557**, 572 (2006).
 - [20] T. Jenke, Ph.D thesis, Vienna University of Technology, 2011.
 - [21] Yu.Yu. Kosvintsev, Nucl. Instr. and Meth. **143**, 133 (1977).
 - [22] J. Feist, A. Bäcker, R. Ketzmerick, S. Rotter, B. Huckestein and J. Burgdörfer, Phys. Rev. Lett. **97**, 116804 (2006); J. Feist, A. Bäcker, R. Ketzmerick, J. Burgdörfer and S. Rotter, Phys. Rev. B **80**, 245322 (2009).
-